Nanoscale

PAPER

View Article Online
View Journal | View Issue

Cite this: *Nanoscale*, 2025, **17**, 19870

Sustainable nanomanufacturing: two-dimensional materials transfer using a bioderived and biodegradable supportive polymer†

Md Arifur Rahman Khan, [a] Swapna Kalkar,[a] Besan Khader, [a] Olubunmi O. Ayodele, [a] Aleksandrs Prokofjevs*[b] and Tetyana Ignatova *[a]

Current methods for transferring 2D materials typically rely on non-biodegradable support polymers, which have a detrimental impact on the environment due to the extensive use of solvents required for polymer removal and the introduction of transfer-induced defects. In this study, we present an approach for synthesizing a biodegradable polyester, poly-angelica lactone (PAL) derived from bio-based raw materials, angelica lactone (α-AL). The biodegradability of the synthesized PAL is activated through a specific mechanism, which has been validated by FTIR and ^{1}H NMR. The molecular weight and thermal properties of PAL have been characterized using GPC and DSC techniques, respectively. We employed PAL as a support layer for the transfer of 2D materials, such as graphene, demonstrating that the removal of PAL requires less than 30 min. The transferred graphene exhibited superior quality compared to conventional PMMA-based methods, with induced strain and doping levels maintained well below ±0.5% and 0.5×10^{12} e cm^{-2}, respectively. Remarkably, the PAL support layer can be efficiently removed from graphene films using a fungus (*e.g.* yeast). This innovative approach not only emphasizes the eco-friendly nature of the process but also highlights its potential for enabling sustainable and efficient 2D materials transfer, paving the way for greener nanodevice fabrication methods.

Received 24th March 2025,
Accepted 21st July 2025

DOI: 10.1039/d5nr01206f

rsc.li/nanoscale

Introduction

Two-dimensional materials exhibit immense potential across various applications, including new generations of semiconductor devices, quantum computing, electrochemical sensors, *etc*.[1–14] Over the past decade, the top-down approach for fabricating 2D materials, such as mechanical exfoliation, has emerged as a well-established and straightforward technique. However, this method generally yields small-size flakes,[15] thus limiting its applicability[16–18] when larger area samples are required for electronic devices, sensor platforms, and other applications.[19,20] Consequently, the manufacturing of large-area, high-quality monolayer or bilayer samples typically involves chemical vapor deposition (CVD).[21,22]

The CVD process requires an appropriate growth surface, such as Cu or Ni, on which the graphene film is grown. Subsequently, the graphene film is carefully transferred onto an application-specific target substrate,[23] which could be SiO_2/Si,[24] glass,[25] paper,[26] or flexible polymers.[27] Transfer of CVD-grown graphene and other 2D materials is greatly facilitated using sacrificial polymer support. Historically, poly(methyl methacrylate) (PMMA) has held a predominant position as the preferred temporary supporting material for transferring 2D materials in device fabrication.[28] PMMA has proven to be effective in transferring large-scale, high-quality 2D materials,[29] and has also been widely used as resist in lithography process, including e-beam lithography.[30] Currently, there is no viable substitute for PMMA in industrial-scale production, underscoring its value in established processes.

Current research efforts seek to assess alternative transfer support materials,[31–33] such as polystyrene,[34] polycarbonate,[35] paraffin,[36] and polymer blend,[33] to ensure the high quality of transferred films.[36–44] The quest for alternative transfer materials and techniques mandates addressing potential sample contamination by residual components of the polymeric substrate.[45–47] Notably, most of the polymers used in this sector, including the widely used PMMA, fall under the category of non-biodegradable materials. Furthermore, substantial amounts of solvent waste generated during fabrication may carry significant environmental implications. In the realm of contemporary technological challenges, one prominent

[a]*Department of Nanoscience, Joint School of Nanoscience and Nanoengineering, University of North Carolina at Greensboro, NC, USA. E-mail: t_ignato@uncg.edu*
[b]*Department of Chemistry, North Carolina Agricultural and Technical State University, NC, USA. E-mail: aprokofjevs@ncat.edu*

† Electronic supplementary information (ESI) available. See DOI: https://doi.org/10.1039/d5nr01206f

issue revolves around the compatibility of biodegradable materials within industrial settings, ensuring that they effectively serve their intended production purposes.

Poly-angelica lactone (PAL) synthesized from levulinic acid (LA), are considered an excellent potential substitute for currently used polymers (*e.g.*, PMMA) in 2D materials transfer. LA is a highly desirable biobased chemical intermediate.[48] Dehydration of LA causes intramolecular condensation, leading to the formation of the readily polymerizable α-angelica lactone (α-AL, 5-methyl-2(3*H*)furanone), a valuable intermediate in the synthesis of commodity chemicals.[49,50] Interestingly, the biodegradability of α-AL polymers varies depending on the polymerization conditions. This stems from the fact that the α-AL monomer possesses two different reactive functional groups relevant for polymerization: the α,β-unsaturated ester, and the lactone. Polymerization involving the C=C bond of the unsaturated ester moiety leads to the formation of the polyolefin chain decorated by lactone units and their derivatives and can be effected using $BF_3{\cdot}Et_2O$ catalyst (product $M_w \sim 800$–900 g mol^{-1}) or UV light.[51,52] The lack of reactive functional groups in the resulting polyolefin backbone makes it resistant to biodegradation.[51]

In contrast, ring-opening polymerization (ROP) involving the lactone subunit leads to the formation of a biodegradable polyester product containing intact C=C bonds (Fig. 1).[51,53–56] This type of polymerization is induced by more selective transesterification catalysts, such as sodium hydroxide ($M_w \sim 840$ g mol^{-1}), sodium *n*-butoxide ($M_w \sim 1120$ g mol^{-1}) or stannous octoate ($M_n \sim 30\,000$ g mol^{-1}).[51,53]

In this study, we demonstrate that biodegradable α-AL polyesters can successfully replace non-biodegradable polymers in nanomanufacturing, *i.e.*, in the fabrication of 2D devices, which brings substantial environmental benefits in their mass production. To this end, we developed a straightforward procedure for synthesizing α-AL polyesters using a minimal amount (1 mol%) of sodium *tert*-butoxide as the catalyst. The resulting biodegradable polymer product exhibited excellent performance in the transfer of 2D materials, such as graphene and MoS_2, onto the target substrate, SiO_2/Si. To demonstrate this, we comprehensively explored transfer conditions employing our biodegradable polymer as the supporting medium. Specifically, we optimized key process parameters in etching and hydrogen bubbling, which are widely recognized for their effectiveness in transferring large, high-quality graphene films. While testing the biodegradability of our samples, we discovered that the polymeric support can be completely digested by yeast, leaving behind pristine graphene films. This remarkable finding not only underscores the eco-friendly nature of our approach but also showcases its potential for developing conceptually new and highly efficient 2D material transfer processes limited solely to biodegradable polymers.

Experimental

Materials

Reagents used in the synthesis of the α-angelica lactone polyesters were purchased from commercial sources and used as received: α-angelica lactone (5-methyl-2(3*H*) furanone, Alfa Aesar, 98%); sodium *tert*-butoxide (*tert*-C_4H_9ONa, Acros Organics, 99%). Molecular sieves (4 Å with indicator, −8 + 12, *ca.* 2 mm beads) were purchased from Thermo Fisher Scientific. Solvents and other conventional reagents were purchased from Sigma-Aldrich. Monolayer graphene grown on Cu substrate by CVD method was purchased from Graphenea. 2D MoS_2 samples was provided by The Pennsylvania State University Two-Dimensional Crystal Consortium – Materials Innovation Platform (2DCC-MIP). For the biodegradability test, we used *Saccharomyces cerevisiae* yeast strain (204722, SK1-can1(r)) from ATCC. Yeast extract, Peptone, Dextrose (YPD) powder, YPD agar were purchased from Sigma-Aldrich to prepare growth medium and agar plates.

Methods

The PAL synthesis reaction was performed in a 3-neck flask placed on a thermostatically controlled sand bath and equipped with a magnetic stirrer and a reflux condenser. Gel permeation chromatography (GPC) was performed using an

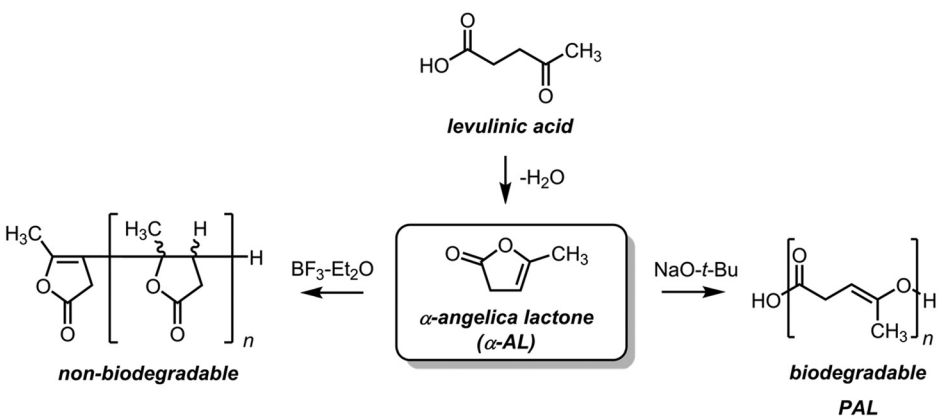

Fig. 1 Idealized structures of α-angelica lactone polymers.

Agilent 1260 Infinity II GPC/SEC instrument equipped with a refractive index detector, using tetrahydrofuran (THF) as the mobile phase. FTIR spectra in the 400–4000 cm^{-1} region were collected using an Agilent 670 FTIR Spectrometer equipped with an ATR attachment. TA Q200 Digital Scanning Calorimeter was used to investigate the response of PAL to heating. Spin-coating was performed by dissolving PAL in an appropriate amount of acetone, which was then applied onto CVD-grown graphene substrates using Laurell EDC-650-8TFM spin processor. Scanning electron microscopy (SEM) was performed using Zeiss Auriga FESEM instrument (5 kV electron beam). Raman spectra and mapping were collected on a WITec alpha300R confocal Raman microscope with a 100× objective lens, using 532 nm laser excitation and 600 g mm^{-1} diffraction grating. Yeast culture growth was monitored by measuring optical density (OD) at 600 nm using a Fisherbrand™ accuSkan™ GO UV/Vis Microplate Spectrophotometer (96-plate well). Biodegradability tests were performed by incubating PAL/graphene/substrate layered samples in the liquid culture of *S. cerevisiae* (Brewer's yeast).

Results and discussion

Synthesis of the α-angelica lactone polyester

The first step in our study was to synthesize the α-AL polyester from the corresponding lactone monomer using sodium *tert*-butoxide (*tert*-C_4H_9ONa) as the catalyst. Prior to polymerization, the α-AL monomer was dried using 4 Å molecular sieves for 72 hours and subsequently transferred into the reaction flask containing a small stirring magnet and the desired amount of the sodium *tert*-butoxide catalyst. The resulting homogeneous mixture was placed on a sand bath heated to 130 ± 4 °C while stirring at 300 rpm. After the indicated time interval, the reaction was terminated by adding an excess of deionized (DI) water to the reaction flask.

Reaction time and catalyst loading significantly impacted the properties of the resulting polymer. The optimum sodium *tert*-butoxide loading was around 1 mol%, while increasing the catalyst loading to 5 mol% led to poor reaction control and difficulties in product isolation. Longer reaction times were observed to deliver higher molecular-weight polyester samples. Consequently, the optimized procedure employs a combination of low catalyst loadings and long reaction times.

To remove water-soluble residues, the crude polymer was washed with 10–20 portions of DI water until the aqueous layer remained clear. Volatile contaminants were removed by dissolving the material in a 70 : 30 acetone : methanol mixture, followed by concentration and drying under reduced pressure at 60 °C for 18 h. Low molecular weight residues were eliminated by dissolving the material in ethyl acetate, followed by selective precipitation of the higher molecular weight fraction by dropwise addition of hexanes. This process also markedly improved the visual appearance of the polymeric material, delivering white or pale-yellow precipitates when a favorable ethyl acetate : hexanes ratio was applied. The purified polymer was finally dried under reduced pressure for 6 hours before characterization and application in graphene transfer. The PAL product is highly soluble in acetone, ethyl acetate and dichloromethane (DCM), partially soluble in methanol and isopropanol, and nearly insoluble in hexanes and water.

PAL characterization. The molecular weight distribution of the polymerization product was evaluated using gel permeation chromatography (GPC). Table 1 shows GPC data for PAL samples obtained after either 1- or 14-day reaction time, before and after precipitation.

After 1 day (24 hours) reaction time, the molecular weights of the crude PAL-1d product are low (M_w 466 g mol^{-1}, M_n 341 g mol^{-1}), although the molar-mass dispersity (PDI) of 1.37 is typical for chain-growth ring opening polymerization.[53,57] Dissolving the crude PAL-1d reaction product in ethyl acetate followed by precipitation with hexanes resulted in a slight increase of the molecular weights (M_w 573 g mol^{-1}, M_n 420 g mol^{-1}), leaving the PDI virtually unchanged (1.36). For this sample, the effect of the reprecipitation was primarily to remove monomer residues, which could not be properly quantified using our GPC setup.

Extending the reaction time to 14 days resulted in a noticeable increase in the polymer chain length (PAL-14d). The GPC analysis of the crude product showed bimodal molecular weight distribution, with the higher molecular weight peak (peak 2 in Table 1) having nearly double M_w value compared to that of the PAL-1d product. To isolate the highest molecular weight fraction from the crude PAL-14d product, the material was dissolved in ethyl acetate and subsequently precipitated with hexanes, as described above. This procedure delivered a sample with M_w 1490 g mol^{-1} and M_n 1007 g mol^{-1}, entirely eliminating the low molecular weight fraction from the purified material. While the purified PAL-14d polymer sample showed a slightly increased PDI value of 1.48, it should be stressed that it is lower than the PDI of 1.8 observed for comparable molecular weight PAL samples reported in ref. 51, and considerably smaller than values seen in commercial polymers.[58]

The purified polymers PAL-1d and PAL-14d were further characterized by FTIR and ^1H NMR spectroscopies. Overall, the spectroscopic data is consistent with the expected formation of the polyester backbone and with previous reports on α-AL ring-opening polymerization.[53] Thus, a comparison of the polymer FTIR spectra with that of the α-AL monomer reveals the presence of the intact C=C double bond in the polymers,

Table 1 GPC results of PAL-1d and PAL-14d before and after purification

Sample		M_w (g mol^{-1})	M_n (g mol^{-1})	PDI
PAL-1d	Crude	466	341	1.37
	Purified	***573***	***420***	***1.36***
PAL-14d	Crude, peak 1	290	277	1.05
	Crude, peak 2	920	757	1.22
	Purified	***1490***	***1007***	***1.48***

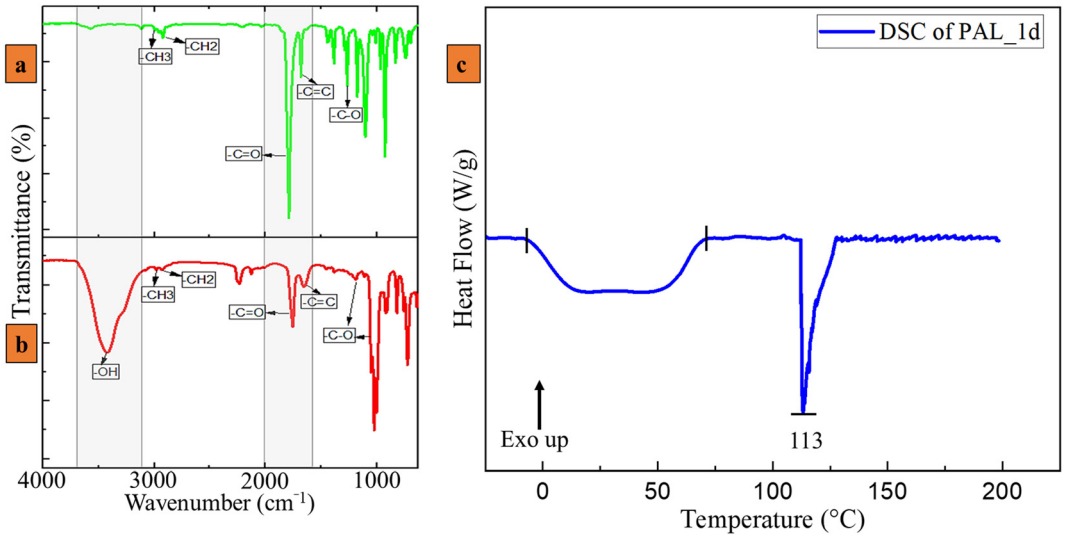

Fig. 2 FTIR spectra of α-angelica lactone, α-AL (a), PAL-1d (b), DSC result of PAL-1d (c).

as well as the expected presence of the C═O groups (Fig. 2a, b; ESI Fig. S2†).

The ^{1}H NMR analysis, however, revealed considerable differences between the previously reported α-AL polyesters and the material prepared in this study (Fig. 3 and ESI Fig. S3†). While both PAL-1d and PAL-14d contain polyester products of the ring-opening polymerization beyond any reasonable doubt, the ^{1}H NMR spectra suggest that the C═C bonds of the product are mostly α,β-conjugated to the ester carbonyl groups. This suggests isomerization of the non-conjugated β,γ-unsaturated ester moiety in the α-AL to the more thermodynamically stable α,β-conjugated form under strongly basic reaction conditions. Furthermore, we also observed the presence of aliphatic fragments reminiscent of the β-AL oligomers produced in the presence of frustrated Lewis pairs.[59] These fragments were also present in the precipitation supernatant obtained upon treatment of the polymer (ESI Fig. S4†). A cautious interpretation of the spectroscopic and GPC data thus suggests that both PAL-1d and PAL-14d samples are low molecular weight AL polyester oligomers that have undergone considerable isomerization to the α,β-unsaturated products while also containing a considerable fraction of the C–C linked AL units.

Differential Scanning Calorimetry (DSC) analysis of PAL-1d revealed significant information regarding the thermal behavior of the polymer, as depicted by the heat flow *vs.* temperature plot in Fig. 2c. The experiment was performed in an inert nitrogen atmosphere in the temperature range of −30 °C to 200 °C. The amorphous nature of the polymer can be assumed by observing the wide range of glass transition temperature (T_g) from −6 °C to 70 °C. Additionally, the DSC curve indicates a unique degradation temperature of the polymer at 113 °C, which might be the melting point. At this stage, the polymer degrades to a phase with a fundamentally different thermal behavior than the initial phase. This crucial insight into the thermal property of the polymer allowed us to optimize the post-transfer heating temperature involved in the graphene transfer method.

Graphene transfer by PAL

There are two extremely popular methods for transferring CVD-grown graphene films: (1) transfer *via* directional etching of growth substrates[60–63] and (2) electrochemical bubble-assisted delamination of the growth substrates.[33,45,64–66] We demonstrate that the α-AL polyester can be successfully used as a supportive polymer layer for both techniques.

The graphene transfer technique using PAL is straightforward as done conventionally, though several steps need to be optimized for a successful transfer. As-purchased CVD-grown graphene was spin coated in two steps by 75 wt% PAL solution in acetone. The spin coating was first performed at 400 rpm for 15 seconds, followed by drying on a hot plate at 70 °C for 30 minutes. The sample was then re-coated at 2000 rpm for 45 seconds, followed by drying at room temperature for 24 hours. The Cu substrate underneath the PAL/graphene was etched away with 0.5 M aqueous $FeCl_3$ solution or delaminated using the hydrogen bubbling method. When using the hydrogen bubbling method, the NaOH solution (25 mM) utilized was 4 times more dilute than what is commonly used in our lab for PMMA-coated graphene transfers.

For both transfer techniques, the PAL/graphene sheet was subsequently washed 3 times in DI water, then scooped onto a desired substrate (SiO_2/Si). The post-transfer heat treatment was done at 60 °C for 25 minutes to remove water trapped between the new substrate and PAL/graphene. The PAL coating was then removed by immersing the PAL/graphene/substrate composite into reagent-grade acetone for 20 minutes, followed by washing with isopropanol, cleaning with DI water, and purging with N_2 gas. The result of this protocol is a layer of graphene deposited onto SiO_2/Si substrate.

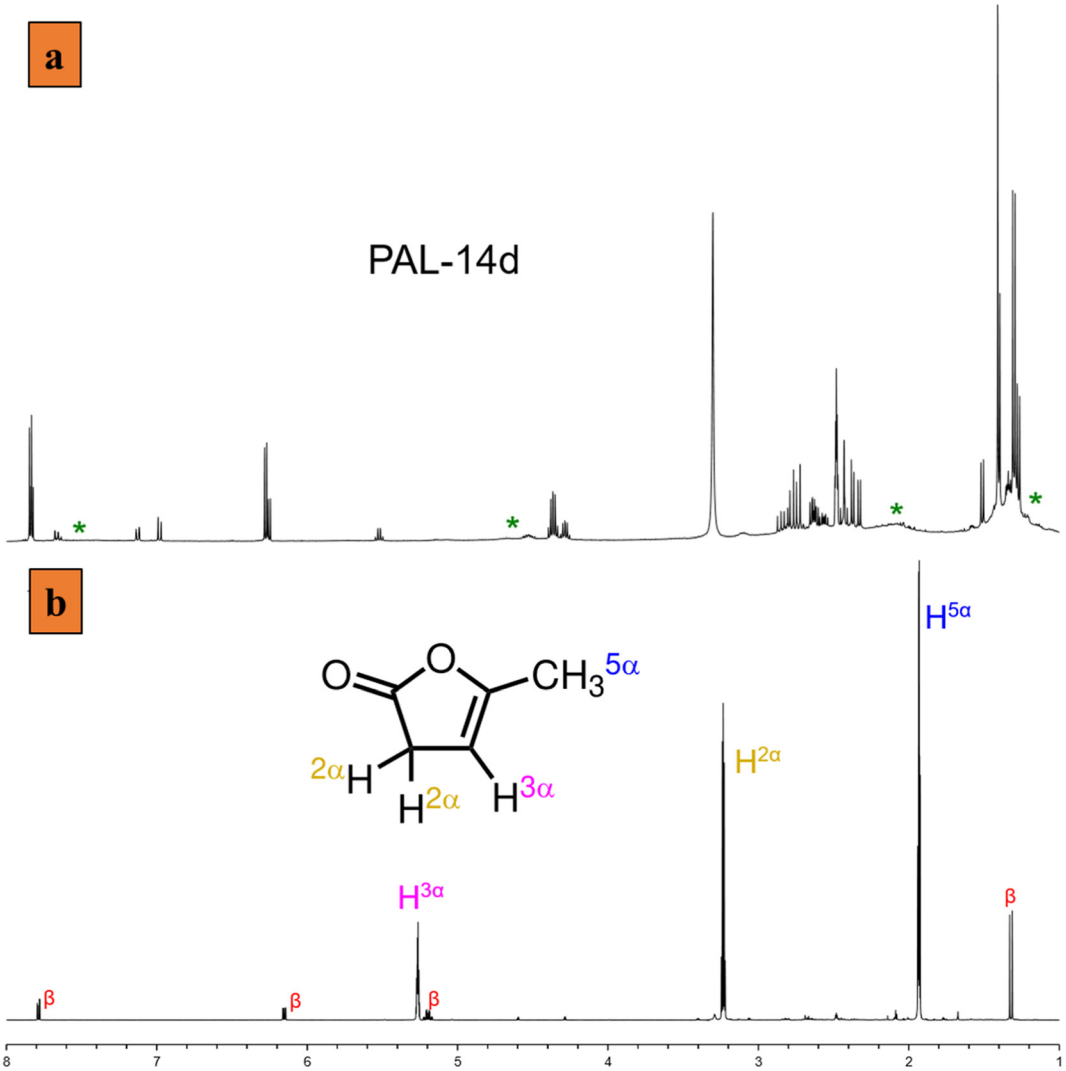

Fig. 3 ^{1}H NMR spectra of (a) PAL-14d and (b) α-AL containing *ca.* 15% of the β-isomer. Note that the PAL-14d spectrum contains broad features (labeled with *) consistent with the previously reported angelica lactone polyesters,[53] and sharp peaks apparently stemming from the previously reported β-AL dimer.[59] Also note that the alkene proton peaks in PAL-14d appear in the same region as the conjugated alkene protons of the β-AL, suggesting considerable double bond migration under basic conditions. A broad peak around 12.2 ppm (not shown) in the PAL-14d spectrum suggests presence of COOH groups.

Unpurified PAL-1d was unsuitable for the bubbling method as the polymer film was breaking down under tension introduced during hydrogen bubble formation. Nevertheless, it proved successful for graphene transfer with the etching method (ESI Fig. S5†), although this method requires additional cleaning of the graphene to remove etchant residues. The bubbling method is generally more popular than etching because it is performed in DI water, improving cleanliness of the transfer. Unpurified PAL-14d was more suitable for the bubbling method, providing good quality graphene transfers that required only 20 minutes immersion of the sample in acetone for polymer removal (ESI Fig. S5†). To test whether insufficient mechanical strength of the unpurified PAL-1d films stems from low molecular-weight contaminants, graphene transfer experiments were repeated using PAL-1d purified by reprecipitation as described above. Noticeably, purified PAL-1d was able to sustain the hydrogen bubble pressure better than the crude polymer, resulting in a good quality graphene monolayer transfer by the bubbling method. Fig. 4 shows SEM images of graphene transferred using purified PAL-1d. Fig. 4a shows a large graphene area (approximately 80 μm × 80 μm) with minimal amounts of residual polymer. It is worth mentioning that edges of the transferred graphene are free from polymer residues and folding that is usually experienced in traditional transfer. Fig. 4b provides a more detailed illustration of the transfer quality at an approximate area of 16 μm × 16 μm. This area reveals high quality transfer with very few wrinkles and microcracks, and almost no residual polymer (hardly one or two spots). Several wrinkles and bi- or tri-layer of graphene are visible that can be formed

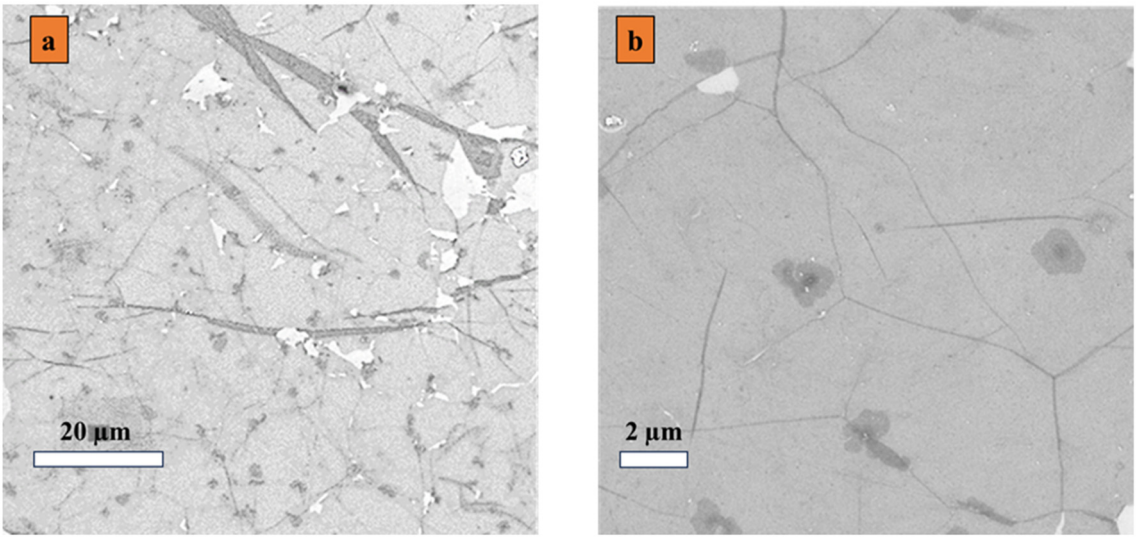

Fig. 4 SEM images of graphene. Transferred by hydrogen bubbling method with clean PAL-1d support (magnification: (a) 1k and (b) 5k).

during either the CVD growth[67] or transfer processes.[68] Transfer-related multilayers are usually formed near the cracks or edges by a folding mechanism with an irregular shape and no geometrical orientation, as the surroundings are extremely variable. Here, we see that the multilayer (bi- or tri-layer) is formed on the top of the perfect monolayer, exhibiting a homogenous geometry. This kind of formation is only probable if the sample is experienced with a homogenous environment, as is possible in the controlled surroundings of the CVD growth process. Thus, we attribute this bi-, or tri-layer formation to the CVD growth process and not to the transfer procedure. It is worth mentioning that polymer removal in our process is complete in under 30 minutes, while conventional PMMA-based transfers often require 3 to 5 hours.[45,69] Additionally, the new procedure is more straightforward compared to the traditional transfer which requires additional steps for polymer removal.[33,45,70]

Raman characterization of transferred graphene

We conducted a point-by-point micro-Raman characterization of a 15 μm × 15 μm area to evaluate the properties of transferred graphene (Fig. 5). Raman spectroscopy is a well-established characterization technique for evaluating the structural and electronic properties of 2D materials, especially graphene. Raman spectra were fitted with Gaussian functions for D, G, and 2D Raman bands in graphene and intensity, peak frequency, and full width at half maximum (FWHM) were extracted as previously reported in ref. 10 and 71. The heat maps of D, G, and 2D Raman peak intensities (using the same scale) revealed a homogeneous distribution over a sufficiently large area, with minor variations present (Fig. 5d–f). Intensity variations are visible in the heat maps in the regions with bi- or tri-layers of graphene and wrinkle or fold formation and correlate perfectly with the optical image shown in Fig. 5a.

In the analyzed area, the G and 2D Raman bands of graphene appeared around 1584.15 cm^{-1} and 2676.17 cm^{-1}, respectively (Fig. 5b). The D Raman band of graphene emerged only at multilayer and wrinkle regions, with I_D/I_G ratios of 0.16 and 0.21, respectively (Fig. 5b and c). The I_{2D}/I_G intensity ratio was 1.29 for the multilayer and 2.41 for the wrinkle regions, compared to 2.53 for the monolayer. Additionally, the 2D peak exhibited a blue shift to 2687.74 cm^{-1} at the multilayer region, while its FWHM broadened to 37.48 cm^{-1}, compared to 32.85 cm^{-1} for the monolayer.

The frequency correlation plot of the G and 2D bands is a reliable technique for evaluating strain and doping in transferred graphene.[10,33,45,71,72] We analyzed and plotted approximately 3600 data points, as shown in Fig. 6a. The solid blue line corresponds to the 2.2 slope line axis for uniaxial (hydrostatic) strain, as reported in ref. 10, 73 and 74. The green solid line with a slope of 0.55 represents the hole doping axis, which follows a quasi-linearity between the G and 2D frequencies, as reported in ref. 75.

The black star ($\omega_G{}^0$ = 1583 cm^{-1}, $\omega_{2D}{}^0$ = 2678 cm^{-1}) in Fig. 6a corresponds to the G and 2D peak position for strain-free and undoped suspended graphene sample,[78] representing an ideal situation. Our analysis revealed that the PAL-transferred graphene film experiences a slight strain and very weak p-doping, as the fitted data align along the 2.2 slope line (Fig. 6a). Although these data points are distributed over both tensile and compressive strain regions, the overall strain level remains below 0.1%. The calculated p-doping concentration is minimal, less than 1 × 10^{12} e·cm^{-2}, as clearly observed in Fig. 6a. Moreover, the already mentioned I_{2D}/I_G intensity ratio can be used to evaluate doping in graphene, as p-doping increases the G peak intensity, the 2D peak intensity decreases.[78–80] The distribution of the I_{2D}/I_G ratio in Fig. 6e shows an average value of 2.04 ± 0.28, supporting our observation of low p-doping of graphene from the correlation plot

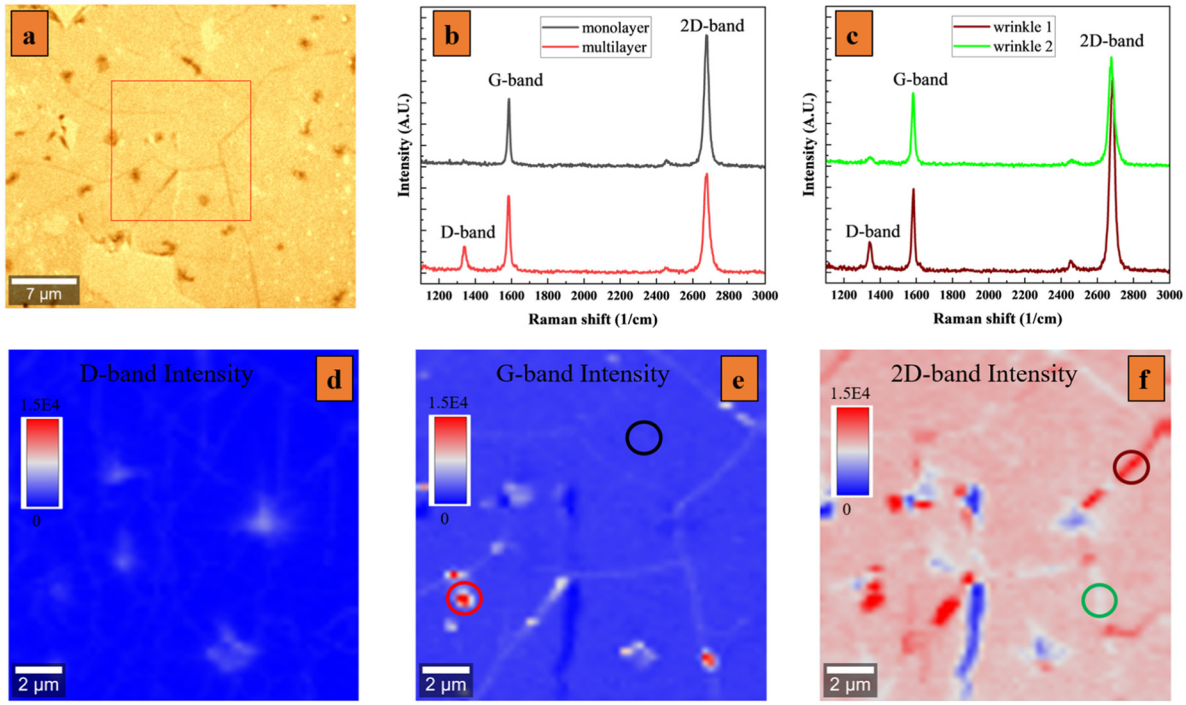

Fig. 5 (a) Optical image of graphene transferred using the PAL-supported bubbling method. The red square marks the area analyzed by Raman spectroscopy. (b and c) Raman spectra collected from monolayer, multilayer, and wrinkled graphene regions. (d–f) Raman intensity heat maps (15 μm × 15 μm) of the main graphene bands. Colored circles indicate the locations where the corresponding spectra in (b) and (c) were acquired.

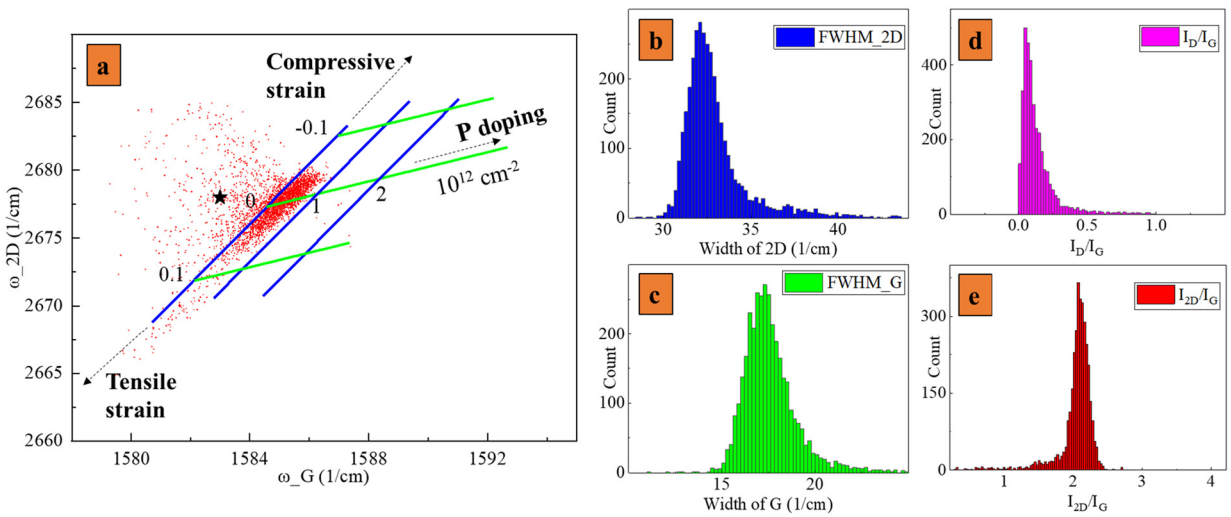

Fig. 6 Frequency correlation plot of G and 2D Raman modes (a). Yoon *et al.*'s work[76] was used to calculate the uniaxial strain-sensitivity of the G mode, which was derived as $\Delta\omega_G/\Delta\omega_\varepsilon = -23.5\ cm^{-1}/\%$. Shifting of the 2D peak at a rate of 1.04 cm^{-1} per 1 × 10^{12} e cm^{-2} hole density has been used for parameterizing the p doping axis as reported in ref. 77. FWHM distribution of 2D peak (b) and G peak (c), intensity ratio of I_D/I_G (d) and I_{2D}/I_G (e).

(Fig. 6a). The FWHM distribution across the entire Raman mapping area further indicates a high-quality graphene transfer, with an FWHM of 17.58 ± 1.43 for the G peak (Fig. 6c) and 32.91 ± 1.83 for the 2D peak (Fig. 6b). The low standard deviation in the G peak width is expected, as the G peak is more sensitive to doping than the 2D peak,[75,77,78,81] aligning with the observed low doping effect in the correlation plot (Fig. 6a). This extended analysis suggests that our PAL-assisted transfer introduces negligible perturbations to the graphene surface, resulting in a high-quality transferred material.

In addition to graphene, MoS_2, a member of the transition metal dichalcogenide (TMDC) family, is a widely recognized 2D material. In this study, we successfully transferred a MOCVD-grown MoS_2 monolayer from a sapphire substrate to a

SiO_2/Si substrate using PAL as a supportive layer. SEM images confirmed the transferred monolayer, and its optoelectronic properties were characterized by photoluminescence (PL) and Raman spectroscopy (ESI Fig. S9†). Further details on PAL-MoS_2 transfer are provided in the ESI.†

Biodegradability test

Following previously developed method,[82] the PAL support layer was removed from graphene using a fungus (*e.g.* yeast). To evaluate the biodegradability of PAL, a small aliquot of yeast culture grown as solid colonies on a YPD agar medium Petri dish was added to 25 mL of liquid YPD medium prepared under laboratory conditions. In a shaking incubator, the culture was grown overnight in 250 mL Erlenmeyer flasks at 30 °C under constant agitation at 100 rpm. After 24 hours, the culture was centrifuged in a Falcon tube, and the supernatant, the liquid YPD medium, was removed. The remaining cells were washed with DI water to obtain an aqueous suspension of pure microbial culture of *S. cerevisiae* (yeast).

PAL spin-coated on graphene/copper was transferred onto a SiO_2/Si substrate using the previously described bubbling method. Following an initial optical microscopy imaging step, the PAL/graphene/SiO_2/Si composite was incubated in a liquid suspension of *S. cerevisiae* and maintained at 30 °C with constant shaking at 100 rpm. To observe the gradual degradation of PAL, the sample was gently rinsed with DI water, air-dried, and imaged every 24 hours. This process was repeated continuously for 33 days, with the liquid suspension of *S. cerevisiae* renewed every 7 days. On the final day, another optical microscopy image was taken (Fig. 7b) and compared with the initial one (Fig. 7a). Fig. 7b shows that the yeast almost completely removed PAL, while Fig. 7c confirms the exposure of graphene under an optical microscope, with only minor PAL residue remaining. It is important to note that the sample was

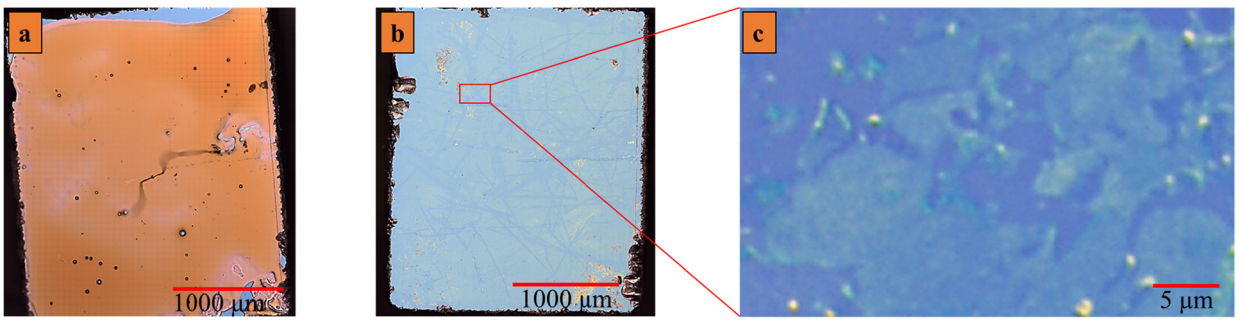

Fig. 7 Optical images of the PAL-1d/graphene/SiO_2/Si before incubation with *S. cerevisiae* (a), and 33 days later (b); higher magnification of graphene surface after yeast assisted PAL-1d removal process (c).

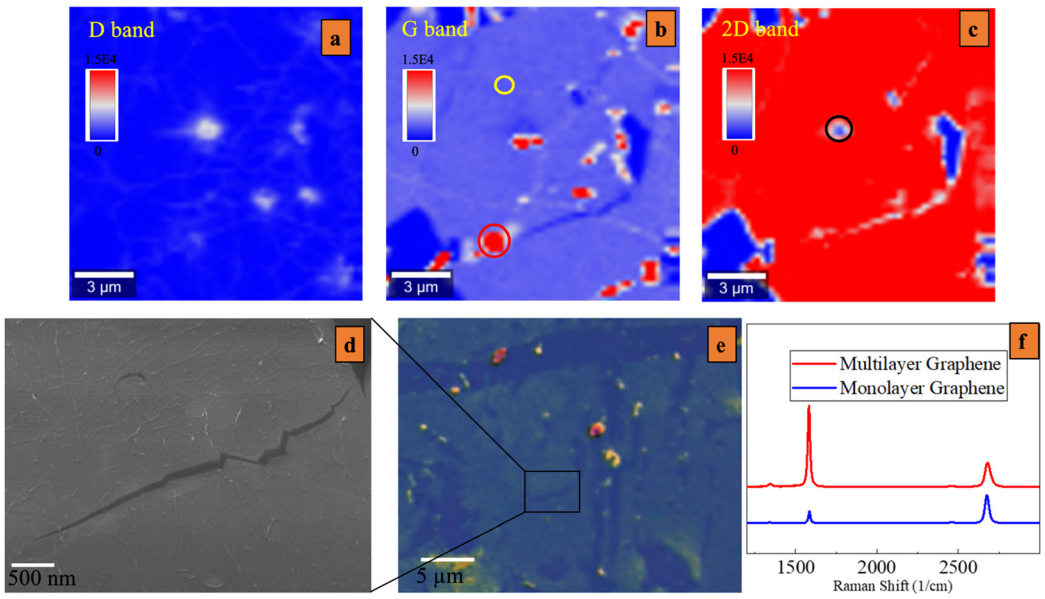

Fig. 8 Raman heat maps of graphene showing D (a), G (b), and 2D (c) band peak intensities. SEM image of graphene exposed after polymer degradation by yeast (d), an optical image indicating the SEM image location (e). Raman spectra were collected from monolayer graphene (yellow circle in b) and multilayer graphene (black circle in b) (f).

only rinsed with DI water; thus, some minor residue of PAL was expected. Additional images and details on the daily degradation process of PAL by yeast can be found in the ESI (Fig. S6†).

Experimental observations suggest that PAL was completely removed well before the 33-day mark. Additionally, a point-by-point micro-Raman characterization was performed on a 15 μm × 15 μm area to obtain more concrete evidence of PAL biodegradation and graphene exposure. Fig. 8e shows the approximate area where Raman and SEM analyses were conducted. The heat maps of the D, G, and 2D bands (with the same color scale), shown in Fig. 8a, b, and c, respectively, confirm the exposure of high-quality graphene.

Color variations in a few spots are primarily attributed to multilayer graphene, as shown in Fig. 8f (red spectrum) for the red-circled spot in the G band heat map, along with minor PAL residues (black-circled spot in the 2D band heat map). These residues persisted due to the absence of vigorous washing, as the sample was only gently rinsed with DI water. More rigorous washing or additional treatments were intentionally avoided to focus exclusively on the yeast-assisted degradation of PAL. To further confirm PAL biodegradation and the environmentally friendly, yeasted-assisted graphene transfer, an SEM image was acquired (Fig. 8d). Additionally, we transferred graphene using PAL-14d as a supportive layer and confirmed its biodegradability through optical microscopy, SEM imaging, and Raman analysis (ESI Fig. S7†).

Conclusion

In summary, we have demonstrated that biodegradable PAL polyesters serve as excellent supports for the high-quality, large area transfer of 2D materials such as graphene and are suitable with multiple transfer methods (Fig. S8†). The graphene film transferred using this new polyester exhibits a low I_D/I_G ratio, reduced strain, and negligible doping compared to conventional polymer-based transfers. The polymerization process, initiated with α-AL and catalyzed by sodium *tert*-butoxide, yields a ring-opened polymeric product with intact C=C double bonds, as confirmed by FTIR and ^{1}H NMR analysis. Notably, PAL synthesis is completed within 24 hours without requiring specialized equipment, and post-transfer PAL removal is significantly faster than conventional methods. We have conclusively shown that PAL's biodegradability allows efficient PAL removal, facilitating a yeast-assisted green transfer of 2D materials – the first such example, to the best of our knowledge. The high quality of the transferred 2D material *via* the yeast-assisted PAL removal protocol was confirmed using optical microscopy, Raman spectroscopy, and SEM imaging. Furthermore, given the advantages of this new PAL-based transfer approach, we have adopted it as our lab's default 2D material transfer protocol. Lastly, this study highlights the potential of biodegradable polymers for photo- and electron beam lithography, opening new research fields for environmentally sustainable fabrication processes.

Conflicts of interest

There are no conflicts to declare.

Data availability

All data needed to evaluate the conclusions in the paper are present in the paper and/or the ESI.† Any additional datasets, analysis details, and sample fabrication recipes are available upon request from the corresponding authors.

Acknowledgements

T. I. and A. K. are grateful for the University of North Carolina System for the UNC ROI Program funding in 2023–2026; T. I., B. K. acknowledge the US Army DEVCOM Soldier Center [Contract #W911QY2220006]. We acknowledge the Pennsylvania State University Two-Dimensional Crystal Consortium—Materials Innovation Platform (2DCC-MIP) which is supported by NSF cooperative agreement DMR-203935. A. P. is grateful AFOSR support: AFOSR grant 21RT0654. This work was performed at the Joint School of Nanoscience and Nanoengineering, a member of the Southeastern Nanotechnology Infrastructure Corridor (SENIC) and National Nanotechnology Coordinated Infrastructure (NNCI), which is supported by the National Science Foundation [ECCS-1542174].

References

1 A. C. Ferrari, *et al.*, Science and technology roadmap for graphene, related two-dimensional crystals, and hybrid systems, *Nanoscale*, 2015, **7**, 4598–4810.
2 K. Parto, S. I. Azzam, K. Banerjee and G. Moody, Defect and strain engineering of monolayer WSe2 enables site-controlled single-photon emission up to 150 K, *Nat. Commun.*, 2021, **12**, 1–8.
3 L. Huang, *et al.*, Graphene/Si CMOS Hybrid Hall Integrated Circuits, *Sci. Rep.*, 2014, **4**, 1–6.
4 Y. H. Wang, K. J. Huang and X. Wu, Recent advances in transition-metal dichalcogenides based electrochemical biosensors: A review, *Biosens. Bioelectron.*, 2017, **97**, 305–316.
5 C. Zhu, D. Du and Y. Lin, Graphene-like 2D nanomaterial-based biointerfaces for biosensing applications, *Biosens. Bioelectron.*, 2017, **89**, 43–55.
6 N. Joshi, *et al.*, A review on chemiresistive room temperature gas sensors based on metal oxide nanostructures, graphene and 2D transition metal dichalcogenides, *Microchim. Acta*, 2018, **185**, 1–16.
7 Z. Sun, A. Martinez and F. Wang, Optical modulators with 2D layered materials, *Nat. Photonics*, 2016, **10**, 227–238.

8 F. Xia, H. Wang, D. Xiao, M. Dubey and A. Ramasubramaniam, Two-dimensional material nanophotonics, *Nat. Photonics*, 2014, **8**, 899–907.
9 S. M. M. Zanjani, M. Holt, M. M. Sadeghi, S. Rahimi and D. Akinwande, 3D integrated monolayer graphene–Si CMOS RF gas sensor platform, *npj 2D Mater. Appl.*, 2017, **1**, 1–9.
10 T. Ignatova, *et al.*, Multidimensional Imaging Reveals Mechanisms Controlling Multimodal Label-Free Biosensing in Vertical 2DM-Heterostructures, *ACS Nano*, 2022, **16**, 2598–2607.
11 S. Goossens, *et al.*, Broadband image sensor array based on graphene–CMOS integration, *Nat. Photonics*, 2017, **11**, 366–371.
12 H. Zhang, Ultrathin Two-Dimensional Nanomaterials, *ACS Nano*, 2015, **9**, 9451–9469.
13 Y. Zuo, *et al.*, Optical fibres with embedded two-dimensional materials for ultrahigh nonlinearity, *Nat. Nanotechnol.*, 2020, **15**, 987–999.
14 N. Zhang, *et al.*, Tuning the Fermi Level of Graphene by Two-Dimensional Metals for Raman Detection of Molecules, *ACS Nano*, 2024, **18**, 8876–8884.
15 K. S. Novoselov, *et al.*, Electric field in atomically thin carbon films, *Science*, 2004, **306**, 666–669.
16 Y. Cao, *et al.*, Unconventional superconductivity in magic-angle graphene superlattices, *Nature*, 2018, **556**, 43–50.
17 K. S. Novoselov, *et al.*, Two-dimensional gas of massless Dirac fermions in graphene, *Nature*, 2005, **438**, 197–200.
18 Y. Zhang, Y. W. Tan, H. L. Stormer and P. Kim, Experimental observation of the quantum Hall effect and Berry's phase in graphene, *Nature*, 2005, **438**, 201–204.
19 Y. T. Li, *et al.*, Rapid and sensitive *in situ* detection of polar antibiotics in water using a disposable Ag–graphene sensor based on electrophoretic preconcentration and surface-enhanced Raman spectroscopy, *Biosens. Bioelectron.*, 2013, **43**, 94–100.
20 D. Akinwande, *et al.*, Graphene and two-dimensional materials for silicon technology, *Nature*, 2019, **573**, 507–518, DOI: 10.1038/s41586-019-1573-9.
21 S. Xu, L. Zhang, B. Wang and R. S. Ruoff, Chemical vapor deposition of graphene on thin-metal films, *Cell Rep. Phys. Sci.*, 2021, **2**, 100372.
22 I. Kandybka, *et al.*, Chemical Vapor Deposition of a Single-Crystalline MoS2 Monolayer through Anisotropic 2D Crystal Growth on Stepped Sapphire Surface, *ACS Nano*, 2024, **18**, 3173–3186.
23 K. Yılmaz, M. Gürsoy, H. Şakalak, M. Ersöz and M. Karaman, Transfer of CVD-Graphene on Real-World Surfaces in an Eco-Friendly Manner, *ACS Appl. Eng. Mater.*, 2023, **1**, 2042–2049.
24 A. Shivayogimath, *et al.*, Do-It-Yourself Transfer of Large-Area Graphene Using an Office Laminator and Water, *Chem. Mater.*, 2019, **31**, 2328–2336.
25 Johnson, *Transfer of monolayer graphene onto flexible glass substrates*, 2015.
26 S. Kumar, S. Kaushik, R. Pratap and S. Raghavan, Graphene on paper: A simple, low-cost chemical sensing platform, *ACS Appl. Mater. Interfaces*, 2015, **7**, 2189–2194.
27 M. Marchena, *et al.*, Dry transfer of graphene to dielectrics and flexible substrates using polyimide as a transparent and stable intermediate layer, *2D Mater.*, 2018, **5**, 035022.
28 A. J. Watson, W. Lu, M. H. D. Guimaraes and M. Stöhr, Transfer of large-scale two-dimensional semiconductors: Challenges and developments, *2D Mater.*, 2021, **8**, 032001.
29 S. Ullah, *et al.*, Graphene transfer methods: A review, *Nano Res.*, 2021, **14**, 3756–3772.
30 L. T. Romankiw, A Path: From Electroplating through Lithographic Masks in Electronics to LIGA in MEMS, *Electrochim. Acta*, 1997, **42**, 2985–3005.
31 M. Nakatani, *et al.*, Ready-to-transfer two-dimensional materials using tunable adhesive force tapes, *Nat. Electron.*, 2024, **7**, 119–130.
32 M. Shang, *et al.*, Polyacrylonitrile as an Efficient Transfer Medium for Wafer-Scale Transfer of Graphene, *Adv. Mater.*, 2024, **36**, 2402000.
33 J. K. Averitt, *et al.*, Efficient high-throughput method utilizing neural network potentials to calculate interaction energies, validated by clean transfer experiment of CVD graphene with polymer mixtures, *Carbon*, 2024, 119336.
34 T. Nasir, *et al.*, Design of softened polystyrene for crack- and contamination-free large-area graphene transfer, *Nanoscale*, 2018, **10**, 21865–21870.
35 X. Yang and M. Yan, Removing contaminants from transferred CVD graphene, *Nano Res.*, 2020, **13**, 599–610.
36 W. S. Leong, *et al.*, Paraffin-enabled graphene transfer, *Nat. Commun.*, 2019, **10**, 867.
37 Y. Chen, X. L. Gong and J. G. Gai, Progress and Challenges in Transfer of Large-Area Graphene Films, *Adv. Sci.*, 2016, **3**, 1500343.
38 A. Ambrosi and M. Pumera, The CVD graphene transfer procedure introduces metallic impurities which alter the graphene electrochemical properties, *Nanoscale*, 2013, **6**, 472–476.
39 H. C. Lee, *et al.*, Review of the synthesis, transfer, characterization and growth mechanisms of single and multilayer graphene, *RSC Adv.*, 2017, **7**, 15644–15693.
40 M. H. Amiri, *et al.*, Doping free transfer of graphene using aqueous ammonia flow, *RSC Adv.*, 2020, **10**, 1127–1131.
41 I. A. Kostogrud, E. V. Boyko and D. V. Smovzh, The main sources of graphene damage at transfer from copper to PET/EVA polymer, *Mater. Chem. Phys.*, 2018, **219**, 67–73.
42 F. Comanescu, A. Istrate and M. Purica, Assessing by Raman spectroscopy the quality of CVD graphene transferred on oxidized silicon and quartz substrates, *Rom. J. Inf. Sci. Technol.*, 2019, **22**, 30–40.
43 F. Comanescu, A. Istrate and M. Purica, Raman Investigation of Critical Steps in Monolayer Graphene Transfer Form Copper Substrate to Oxidized Silicon by Means of Electrochemical Delamination, *Proceedings of the International Semiconductor Conference, CAS*, 2018, vol. 2018-October, pp. 269–272.

44 Y. C. Lin, *et al.*, Recent Advances in 2D Material Theory, Synthesis, Properties, and Applications, *ACS Nano*, 2023, **17**, 9694–9747, DOI: **10.1021/acsnano.2c12759**.
45 O. O. Ayodele, S. Pourianejad, A. Trofe, A. Prokofjevs and T. Ignatova, Application of Soxhlet Extractor for Ultra-clean Graphene Transfer, *ACS Omega*, 2022, **7**, 7297–7303.
46 J. P. Merino, *et al.*, Ethanol Solvation of Polymer Residues in Graphene Solution-Gated Field Effect Transistors, *ACS Sustainable Chem. Eng.*, 2024, **12**, 9133–9143.
47 H. Liu, J. Zhao and T. H. Ly, Clean Transfer of Two-Dimensional Materials: A Comprehensive Review, *ACS Nano*, 2024, **18**, 11573–11597.
48 F. D. Pileidis and M. M. Titirici, Levulinic Acid Biorefineries: New Challenges for Efficient Utilization of Biomass, *ChemSusChem*, 2016, **9**, 562–582.
49 J. Xin, *et al.*, Formation of C-C bonds for the production of bio-alkanes under mild conditions, *Green Chem.*, 2014, **16**, 3589–3595.
50 C. G. S. Lima, J. L. Monteiro, T. de M. Lima, M. W. Paixão and A. G. Corrêa, Angelica Lactones: From Biomass-Derived Platform Chemicals to Value-Added Products, *ChemSusChem*, 2018, **11**, 25–47.
51 V. E. Tarabanko and K. L. Kaygorodov, New Biodedradable Polymers Based on α-Angelicalactone, *Chem. Sustainable Dev.*, 2010, **18**, 321–328.
52 C. S. Marvel and C. L. Levesque, The Structure of Vinyl Polymers. III.1 The Polymer from α-Angelica Lactone, *J. Am. Chem. Soc.*, 1939, **61**, 1682–1684.
53 T. Chen, *et al.*, Degradable polymers from ring-opening polymerization of α-angelica lactone, a five-membered unsaturated lactone, *Polym. Chem.*, 2011, **2**, 1190–1194.
54 V. A. Fomin and V. V. Guzeev, Biodegradable Polymers, Their Present State and Future Prospects, *Int. Polym. Sci. Technol.*, 2001, **28**, 76–84.
55 B. V. Lebedev, Russian Academy of Sciences and Turpion Ltd, *Russ. Chem. Rev.*, 1996, **65**, 1063–1082.
56 R. S. Stein, Polymer recycling: opportunities and limitations, *Proc. Natl. Acad. Sci. U. S. A.*, 1992, **89**, 835–838.
57 X. Xi, G. Jiang, X. Wang, R. Hu and R. Wang, Synthesis, Characterization and Degradation Properties of Poly (α-angelica lactone-co-ε-caprolactone) Copolymers, *Polym. Renewable Resour.*, 2013, **4**, 49–60.
58 A. Shrivastava, *Polymerization, in Introduction to Plastics Engineering*, Elsevier, 2018, pp. 17–48.
59 X. J. Wang and M. Hong, Lewis-Pair-Mediated Selective Dimerization and Polymerization of Lignocellulose-Based β-Angelica Lactone into Biofuel and Acrylic Bioplastic, *Angew. Chem., Int. Ed.*, 2020, **59**, 2664–2668.
60 W. Fang, *et al.*, Asymmetric growth of bilayer graphene on copper enclosures using low-pressure chemical vapor deposition, *ACS Nano*, 2014, **8**, 6491–6499.
61 X. Li, *et al.*, Transfer of large-area graphene films for high-performance transparent conductive electrodes, *Nano Lett.*, 2009, **9**, 4359–4363.
62 X. Li, *et al.*, Large-area synthesis of high-quality and uniform graphene films on copper foils, *Science*, 2009, **324**, 1312–1314.
63 D. Y. Wang, *et al.*, Clean-Lifting Transfer of Large-area Residual-Free Graphene Films, *Adv. Mater.*, 2013, **25**, 4521–4526.
64 Y. Fan, K. He, H. Tan, S. Speller and J. H. Warner, Crack-free growth and transfer of continuous monolayer graphene grown on melted copper, *Chem. Mater.*, 2014, **26**, 4984–4991.
65 L. Gao, *et al.*, Repeated growth and bubbling transfer of graphene with millimetre-size single-crystal grains using platinum, *Nat. Commun.*, 2012, **3**, 1–7.
66 Y. Wang, *et al.*, Electrochemical delamination of CVD-grown graphene film: Toward the recyclable use of copper catalyst, *ACS Nano*, 2011, **5**, 9927–9933.
67 H. T. Chin, J. J. Lee, M. Hofmann and Y. P. Hsieh, Impact of growth rate on graphene lattice-defect formation within a single crystalline domain, *Sci. Rep.*, 2018, **8**, 1–6.
68 P. V. Pham, *et al.*, Transfer of 2D Films: From Imperfection to Perfection, *ACS Nano*, 2024, **18**, 14841–14876, DOI: **10.1021/acsnano.4c00590**.
69 Z. Wang, *et al.*, Germanium-Assisted Direct Growth of Graphene on Arbitrary Dielectric Substrates for Heating Devices, *Small*, 2017, **13**, 1700929.
70 G. B. Barin, *et al.*, Optimized graphene transfer: Influence of polymethylmethacrylate (PMMA) layer concentration and baking time on grapheme final performance, *Carbon*, 2015, **84**, 82–90.
71 K. Schmidt, A. Trofe and T. Ignatova, Communication–Multimodal Image Correlation in Two-Dimensional Materials via Automated Image Processing by Strain and Doping Analysis, *ECS J. Solid State Sci. Technol.*, 2022, **11**, 121007.
72 B. Ying, *et al.*, Efficient Charge Transfer in Graphene/CrOCl Heterostructures by van der Waals Interfacial Coupling, *ACS Appl. Mater. Interfaces*, 2024, **16**, 43806–43815.
73 N. S. Mueller, *et al.*, Evaluating arbitrary strain configurations and doping in graphene with Raman spectroscopy, *2D Mater.*, 2018, **5**, 015016.
74 J. E. Lee, G. Ahn, J. Shim, Y. S. Lee and S. Ryu, Optical separation of mechanical strain from charge doping in graphene, *Nat. Commun.*, 2012, **3**, 1024.
75 G. Froehlicher and S. Berciaud, Raman spectroscopy of electrochemically gated graphene transistors: Geometrical capacitance, electron-phonon, electron-electron, and electron-defect scattering, *Phys. Rev. B:Condens. Matter Mater. Phys.*, 2015, **91**, 205413.
76 D. Yoon, Y. W. Son and H. Cheong, Strain-dependent splitting of the double-resonance raman scattering band in graphene, *Phys. Rev. Lett.*, 2011, **106**, 155502.
77 A. Das, *et al.*, Phonon renormalization in doped bilayer graphene, *Phys. Rev. B:Condens. Matter Mater. Phys.*, 2009, **79**, 155417.
78 A. Das, *et al.*, Monitoring dopants by Raman scattering in an electrochemically top-gated graphene transistor, *Nat. Nanotechnol.*, 2008, **3**, 210–215.

79 S. Zhao, S. P. Surwade, Z. Li and H. Liu, Photochemical oxidation of CVD-grown single layer graphene, *Nanotechnology*, 2012, **23**, 355703.
80 D. M. Basko, S. Piscanec and A. C. Ferrari, Electron-electron interactions and doping dependence of the two-phonon Raman intensity in graphene, *Phys. Rev. B:Condens. Matter Mater. Phys.*, 2009, **80**, 165413.
81 M. Bruna, *et al.*, Doping dependence of the Raman spectrum of defected graphene, *ACS Nano*, 2014, **8**, 7432–7441.
82 T. Ignatova, O. O. Ayodele and S. Kalkar, Novel Methods of Removing a Sacrificial Polymer in Polymer-Assisted Graphene Transfer; and Novel Bacillus Megaterium Strains, Related Compositions and Methods. *U.S. Patent Application* 18379157, 2024.